Detailed Modeling of Stationary and Transient Mass Transfer Across Pervaporation Membranes

Jürgen Bausa and Wolfgang Marquardt
Lehrstuhl für Prozesstechnik, RWTH Aachen, D-52056 Aachen, Germany

The slow dynamic behavior of mass transfer in pervaporation has been reported by different authors. Until now, however, only a little experimental data and no model capable to describe this phenomenon have been available. A new detailed model for mass transfer in pervaporation, based on the dual-sorption theory, Maxwell-Stefan diffusion, and the UNIQUAC model, is proposed. This model is capable of properly describing mass transfer at steady state and during transients. Model parameters for two different PVA/PAN membranes for ethanol/water separation are given. The model shows good agreement with both steady state and dynamic experimental data.

Introduction

In the last decades, the search for alternatives to traditional but energy-intensive separation methods like distillation has led to processes based on membranes. In particular, pervaporation processes can be an alternative for separations that are typically done by distillation. Pervaporation is a membrane process where the components change their aggregate state from liquid to vapor while permeating. Due to the needed vacuum equipment it is a costly process with a high-energy demand compared to other membrane techniques. However, its energy demand is small when compared to distillation, and in many cases pervaporation is an economical alternative (Rautenbach and Albrecht 1985a,b). In the last decades pervaporation membranes have been developed for many purposes. Thus, specific membrane types are available for many applications. Many case studies indicate that the best application of pervaporation is as part of a hybrid process (Moganti et al., 1994; Pettersen and Lien, 1995; Pressly and Ng, 1998; Bausa and Marquardt, 2000).

Today modeling and numerical simulation of chemical engineering processes is widespread in the process industries. For many processes models are available through simulators like ASPEN PLUS, PRO/II, or HYSYS. However, these simulators provide steady-state models only. While steady-state models can be applied in process design, dynamic models are needed to investigate aspects of process control, disturbance rejection, or optimization of process transients (such as startup optimization). Consequently, dynamic modeling has received an increasing interest in the last decade (Helget et al., 1994).

Correspondence concerning this article should be addressed to Jürgen Bausa.

While in the field of distillation, for example, modeling and simulation are widespread and steady-state and dynamic models are available on different scales (models for VLE, mass transfer, tray hydraulics, or whole columns), the detailed modeling of membrane processes has attracted comparatively little interest. Often, empiric models are fitted to experimental data for one special membrane (Vier, 1995). And even detailed models (Heintz and Stephan, 1994a,b) cover steady-state conditions only. However, for the integrated design of pervaporation plants, which covers aspects of feasibility, economics, and control, not only steady-state, but also dynamic models are needed. In particular pervaporation processes are known to exhibit a very slow dynamic behavior, and it may take several minutes or hours in order to reach steady state (Ping et al., 1988). This phenomenon has been reported by different sources as a problem when measuring steady-state fluxes. In most cases, only qualitative information is available. Recently, quantitative dynamic experimental data have been published by Rautenbach and Hömmerich (1998). These data show that the dominant time constant of the mass transfer through the membrane has the same order of magnitude as the dominating time constant of the membrane separator, when modeled with a steady-state mass-transfer model (Hömmerich et al., 1998). Thus, it is clear that mass-transfer dynamics will affect the dynamic behavior of the whole process and must not be neglected.

In this work a detailed, mechanistic, and physically motivated model for the mass transfer through pervaporation membranes is developed. The model is based on dynamic balances and a description of diffusional fluxes by the

Maxwell-Stefan equations (Taylor and Krishna, 1993). In addition, the dual-sorption theory (Vieth et al., 1975) is used to describe the slow sorption/swelling behavior of the membrane. These assumptions lead to a system of partial differential algebraic equations (PDAE). Experimental data from the literature is used to fit the unknown parameters of the model. In the section titled ''Simulation Results,'' simulation studies are used to show the dynamic behavior of the model. In addition, the model is compared to experimental steady-state and dynamic data from the literature.

Model Formulation

The membranes that are considered here are known to exhibit strong swelling when in contact with a swelling agent like water. Since it is also known that the swelling state has a strong influence on the diffusion process, it must be considered when modeling mass transfer across membranes.

Swelling and its impact on the diffusion process have been addressed by different authors. Eaton et al. (1975) address equilibrium properties of swollen hydrophilic membranes in a liquid phase in the presence of salts. Peppas and Moynihan (1985) develop a theoretical model to describe solute transport through moderately swollen polymer networks. This model takes the effect of the swelling state at equilibrium on the diffusional fluxes into account. Devotta et al. (1994) use *in situ* NMR measurements of the dynamic swelling–dissolution process in a rubbery polymer. Based on the microscopic observations, a mathematical model for the swelling–dissolution process is developed that treats the swelling process and the dissolution process as distinct decoupled processes.

In the approach presented here, these ideas are transferred to the dynamic modeling of mass transfer through membranes. The dynamic swelling and diffusion process is modeled with the use of the dual-sorption theory (Vieth et al., 1975). According to the dual-sorption theory, there are two different physical mechanism that affect mass transfer: diffusion and embedding. While the diffusion process is fast, the embedding process is relatively slow. Both processes are linked, since the diffusion coefficients depend on the number of molecules embedded in the polymer structure of the membrane. This phenomena can be explained by the idea of molecules embedded in the polymer structure that are widening the interspace between the polymer chains, which facilitates the diffusion of the permeating molecules.

If a change occurs in the state on the feed side, the activity of the feed changes, directly affecting the driving force for diffusion. This change will result almost immediately in a change in the fluxes. However, the swelling state is also affected, but will change slowly. Thus, after the fluxes have changed very fast due to the change in the driving forces, the swelling state will be nearly the same as before, plus the diffusion coefficients won't have changed. Now the membrane begins to change its swelling state slowly, which will affect the diffusion coefficients and thus the fluxes again. Through this mechanism the fluxes will change in two steps.

Figure 1 depicts the structure of the presented model based on the methodology proposed by Marquardt (1995). The membrane is split up into two modeling components, the active layer and the porous supporting layer. The active layer is represented by two phases that correspond to the two modes of sorption as proposed by the dual-sorption theory. Additional modeling components represent the porous supporting layer, the feed phase, and the permeate phase at the back side of the membrane. These modeling components are linked by the boundary conditions and fluxes between them. In the following, we present models to describe the modeling components and their connections.

Active layer

The main idea of the dual-sorption theory is that a permeating molecule can have two different modes: similar to a molecule dissolved in a fluid, it can be *dissolved*, or, when the molecule is ''caught'' in the polymer structure, it can be embedded. Diffusion occurs only in the dissolved mode. However, there is an exchange between the two modes. In the following, the different modes are regarded as different phases.

These ideas are transferred to the active layer of a pervaporation membrane (Figure 2). When a mixture of two components, for example, ethanol and water, permeates through

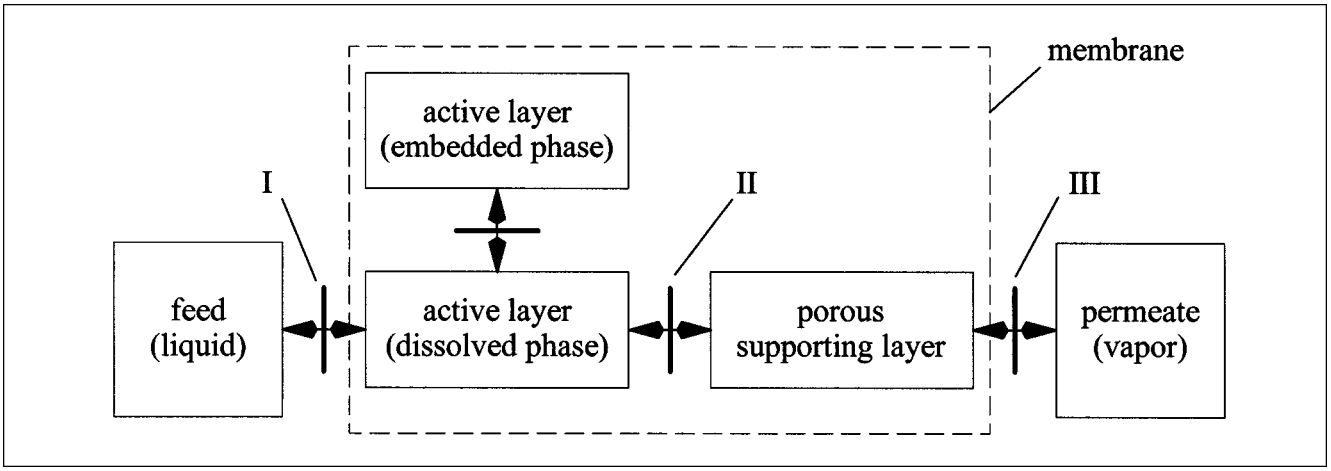

Figure 1. Model structure.

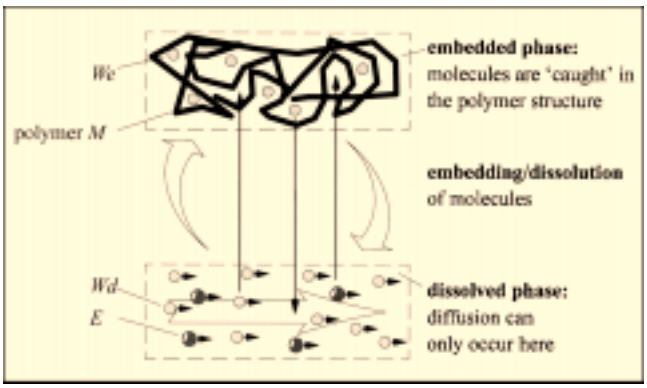

Figure 2. Dual-sorption model for mass transfer in the active layer of a pervaporation membrane.

the membrane M, four species must be balanced, as shown in Table 1.

Balances

The following system of equations is obtained from general balances, if one-dimensional fluxes are assumed only:

$$\frac{\partial(w_i \rho_t)}{\partial t} = -\left(\frac{\partial(w_i n_t)}{\partial z} + \frac{\partial j_i}{\partial z}\right) + r_i$$

$$\text{with} \quad i \in \{E, Wd, We, M\}. \quad (1)$$

Here r_i is the flux of embedding and dissolution, n_t is the total mass flux, j_i is the diffusive flux of component i; w_i is the mass fraction of component i; z is the spatial coordinate; and t is the time. Formulations for the fluxes will be given in the following.

In the case of pervaporation, not only mass but also heat has to be transferred across the membrane in order to evaporate the permeating components on the back side of the membrane. Since a temperature gradient across the membrane is necessary to allow heat transfer, the temperature cannot be uniform across the membrane. Due to the very thin active layer ($\delta \approx 3\ \mu$m), however, the temperature difference across the membrane given by Fourier's law,

$$\Delta T \approx \delta \frac{\partial T}{\partial z} = -\delta \frac{q}{k}, \quad (2)$$

is extremely small, even for a high heat flux q. Consequently, in the following the temperature in the active layer is considered to be constant and equal to the feed and permeate temperature, and no energy balance is needed.

Calculation of fluxes

Embedding/Dissolution Rates. Since ethanol is not embedded and the membrane material is not dissolved, the embedding/dissolution rates for ethanol and the membrane material r_E and r_M are zero. For the water component the rates in both phases are $r_{Wd} = -r_{We}$. To model the process of embedding and dissolution, an expression similar to reaction kinetics or adsorption modeling is chosen:

$$r_{We} = k_W(a_{Wd} - \alpha_{We}). \quad (3)$$

At equilibrium, the activities a_{We} and a_{Wd} are the same and the rate is zero. Thus, k_W is a completely kinetic parameter that has no influence at steady state.

Diffusive Fluxes. To model the diffusive fluxes j, the Maxwell-Stefan equations (Taylor and Krishna, 1993) are applied. Although they were originally meant for liquid systems, they are utilized for a solid phase, the active layer of the membrane, as proposed by Heintz and Stephan (1994a,b). This utilization can be motivated by the applicability of the model ideas that lead to the Maxwell-Stefan equations. Based on the momentum balance, these equations relate the forces acting on the molecules of each species (the gradient of the chemical potential) to the friction between this species and any other species. In our case, one species (the material of the active layer) is the solid phase, which means the molecules are fixed in a matrix structure. However, this fact has no influence on the friction between this species and any other species permeating through the membrane. Note that similar assumptions lead to the dusty-gas model (Mason and Malinauskas, 1983) that describes diffusion in porous media and is typically used in the modeling of gas/solid heterogeneous catalysis.

The general fluxes are

$$d_i = \frac{x_i}{RT}\left(\frac{\partial \mu_i}{\partial z}\right)_{T,p} = -\sum_{k=1}^{C} \frac{x_i x_k (u_i - u_k)}{Đ_{i,k}},$$

$$\text{with} \quad Đ_{i,k} = Đ_{k,i} \quad \text{and} \quad i = 1 \ldots C. \quad (4)$$

However, the material in the active layer of the membrane is a polymer (that is, a mixture of molecules of different chain length) that has no distinct molecular weight. Thus, the composition of the swollen membrane should be described by mass factions, not mol fractions.

Using mass fractions w_i, the Maxwell-Stefan equations become

$$\left(\sum_{j=1}^{C} \frac{w_j}{M_j}\right) \frac{w_i}{RT}\left(\frac{\partial \mu_i}{\partial z}\right)_{T,p} = -\sum_{k=1}^{C} \frac{w_i w_k (u_i - u_k)}{Đ_{i,k} M_k}, \quad i = 1 \ldots C. \quad (5)$$

Inserting the definition of the diffusive fluxes

$$j_i = \rho_i(u_i - v) = \rho_t w_i (u_i - v), \quad (6)$$

the following equations are obtained

$$\left(\sum_{j=1}^{C} \frac{w_j}{M_j}\right) \frac{w_i}{RT}\left(\frac{\partial \mu_i}{\partial z}\right)_{T,p} = -\sum_{k=1}^{C} \frac{w_k j_i - w_i j_k}{\rho_t Đ'_{i,k} M_k},$$

$$i = 1 \ldots C. \quad (7)$$

Table 1. Different Modes of Permeating Molecules

	Dissolved Phase	Embedded Phase
Ethanol	E	—
Water	Wd	We
Membrane	—	M

The chemical potential in the membrane phase can be described by means of an activity coefficient with reference to mass fractions:

$$\mu_i(T, p, w) = \mu_{0,i}(T, p) + RT \ln a_i$$
$$= \mu_{0,i}(T, p) + RT \ln w_i + RT \ln \gamma_i', i = 1 \ldots C \quad (8)$$
$$\gamma_i' = \frac{a_i}{w_i}. \quad (9)$$

Using this formulation, the lefthand side of Eq. 7 gives

$$\frac{w_i}{RT}\left(\frac{\partial \mu_i}{\partial z}\right)_{T,p} = \left(\mathbf{\Gamma}_i \cdot \frac{\partial w}{\partial z}\right), \quad i = 1 \ldots C, \quad (10)$$

where $\mathbf{\Gamma}_i$ denotes the ith row of a matrix $\mathbf{\Gamma}$ with the matrix elements

$$\Gamma_{i,j} = \frac{w_i}{RT}\frac{\partial \mu_i}{\partial w_j} = \delta_{i,j} + w_i \frac{\partial \ln \gamma_i'}{\partial w_j} \quad (11)$$

and the Kronecker delta $\delta_{i,j}$ (1 if $i = j$; 0 if $i \neq j$). Here and in the following the notation of the dot product is taken from append. A of Bird et al. (1960).

Since the molecular weight of the polymer is not known, the term $\sum_{j=1}^{C} (w_j/M_j) = f(w)$ cannot be computed. To remedy this problem, new diffusion coefficients

$$Đ_{i,k}' \equiv Đ_{i,k} M_k \sum_{j=1}^{C} \frac{w_j}{M_j} \quad (12)$$

are introduced to rewrite the Maxwell-Stefan equations (Eq. 7) using Eq. 12:

$$\left(\mathbf{\Gamma}_i \cdot \frac{\partial w}{\partial z}\right) = -\sum_{k=1}^{C} \frac{w_k j_i - w_i j_k}{\rho_t Đ_{i,k}'}, \quad i = 1 \ldots C. \quad (13)$$

Rearranging Eq. 13 and converting the linear set of equations into matrix notation gives

$$-\frac{1}{\rho_t}[B \cdot j] = \left[\mathbf{\Gamma} \cdot \frac{\partial w}{\partial z}\right]. \quad (14)$$

Since only differences of velocities are used in Eqs. 4, no absolute velocities can be calculated from this set of equations. Thus, the scalar equations in Eq. 14 are linearly dependent. In particular, B is singular and cannot be inverted to calculate the fluxes j as a function of the forces. One of the equations in Eq. 14 must be replaced by following equation

$$0 = \sum_{i=1}^{C} j_i, \quad (15)$$

resulting from summation of Eq. 6.

Then, inversion of Eqs. 14 and 15 is feasible and results in

$$j = -\left[D^{GMS} \cdot \frac{\partial w}{\partial z}\right], \quad (16)$$

where the matrix D^{GMS} is a function of the modified Maxwell-Stefan diffusion coefficients $Đ_{i,k}'$ (cf. Eq. 12), compositions w, and temperature T (Taylor and Krishna, 1993).

Supporting layer

The porous supporting layer is a system of capillaries with a wide range of diameters. Due to this wide range and a lack of exact measurements, it is difficult to tell whether the flow in these capillaries is in the Knudsen or convective regime. For simplicity, the porous supporting layer is modeled as a system of identical parallel capillaries with a constant diameter. In these capillaries only convective transport is considered. Since there is no diffusion and the flow is always in the direction from the back side of the active layer (Figure 2, connection II) to the permeate phase (Figure 2, connection III), the permeate phase composition has no influence on the active layer (unhindered permeate flux). Assuming a laminar flow regime in the capillaries gives

$$\frac{dp}{dz} = \frac{8\eta RTN^c}{p\pi r^4}, \quad (17)$$

according to the Hagen-Poiseuille law (Bird et al., 1960).

Integration of this equation across the porous layer results in

$$\frac{1}{2}\left(p_{\mathrm{II}}^2 - p_{\mathrm{III}}^2\right) = \frac{8\eta RTN^c \delta^{SL}}{\pi r^4}, \quad (18)$$

where

$$N^c = \frac{N_t \pi r^2}{\phi} \quad (19)$$

is the molar flow in one capillary, δ^{SL} is the thickness of the supporting layer, ϕ is the area fraction of capillaries in the supporting layer, and η is the viscosity. Now the pressure at connection II can be calculated as

$$p_{\mathrm{II}} = \sqrt{p_{\mathrm{III}}^2 + \frac{16\eta RT\delta^{SL}N_t}{\phi r^2}}. \quad (20)$$

However, values for the parameters (especially ϕ, r, δ^{SL}, η) are difficult to obtain. Since most of them are not known, the parameter

$$K = \frac{16R\delta^{SL}N_t}{\phi r^2} \quad (21)$$

describing the geometric properties of the membrane is introduced. This parameter needs to be determined using a least-square fit for the experimental mass-transfer data available. However, since only little experimental data were avail-

able, the parameter

$$K^{pd} = K\eta T \tag{22}$$

is treated as constant and will be fitted to experimental data in this work.

Boundary conditions

Connection I Between Feed Phase and Active Layer. In this work, only the phase interface between the liquid phase and the active layer, but not the liquid phase itself, is addressed. Thus, concentration polarization is not considered. However, if an appropriate model is available, it could be used to determine the liquid composition at the interface as a function of the bulk feed composition and the flux.

At the interface between the liquid-feed phase and the active layer of the membrane equilibrium for the permeating species (E, Wd) is assumed. This results in two boundary conditions:

$$a_E^L(w_F, T) = a_E^M(w_\mathrm{I}, T), \tag{23}$$

$$a_W^L(w_F, T) = a_{Wd}^M(w_\mathrm{I}, T). \tag{24}$$

Connection II Between Active Layer and Supporting Layer. At the interface between the active layer and the porous supporting layer equilibrium for both permeating species is assumed:

$$a_E^M(w_{\mathrm{II},} T) = a_E^V(y_\mathrm{II}, T, p_\mathrm{II}), \tag{25}$$

$$a_{Wd}^M(w_{\mathrm{II},} T) = a_W^V(y_\mathrm{II}, T, p_\mathrm{II}). \tag{26}$$

The model of the porous supporting layer implies unhindered permeate flux. Thus, the vapor composition at interface II, being in equilibrium with the active layer at $z = \delta$, is equal to the ratio of the fluxes of the two components. Hence,

$$y_{\mathrm{II},i} = \frac{N_i}{N_t}, \tag{27}$$

$$N_i = \frac{\bar{n}_i}{M_i}, \tag{28}$$

where $\bar{n}_i$ is the *true* diffusional flux, that is, the diffusional flux relative to the membrane, which is identical to the desorption rate at interface II (cf. Eq. 66). The Maxwell-Stephan equations to calculate these fluxes are given in the section titled ''Model Transformation and Solution Method.''

Since the fluxes depend on the gradient of the composition inside the active layer, this results in a nonlinear boundary condition of the form $F(w, \partial w/\partial z) = 0$.

Connection III Between Supporting Layer and Permeate Cell. At the interface between the porous supporting layer and the permeate cell, pressure is set to the given permeate pressure:

$$p_\mathrm{III} = p_P. \tag{29}$$

Physical properties

Activities in the Membrane Phase. To calculate the matrix D^{GMS} (cf. Eq. 16), a model for the activity of the components in the membrane is needed. In addition, activities are also needed to describe boundary conditions where equilibrium is assumed (see the section titled ''Boundary Conditions'').

Heintz and Stephan (1994a) use a modified UNIQUAC model to describe activity coefficients in the membrane phase. However, in contrast to, for example, two liquid phases being in equilibrium (LLE case), one component (the material of the active layer) cannot cross the phase interface. In the LLE case, a pure component ($w_j^\mathrm{I} = 1$, $w_{i\neq j}^\mathrm{I} = 0$) on one side of the interface (phase I) will always be in equilibrium with the same composition on the other side (phase II) of the interface: $w^\mathrm{II} = w^\mathrm{I}$. In contrast to this behavior, a pure component on the liquid side of the feed-phase/active-layer interface will be in equilibrium with a composition of the membrane phase, where $w_M \neq 0$ and $w_j < 1$, since the mass fraction of the membrane material cannot become zero. Liquid/gel systems have the same property: Even if the liquid is a pure component, the mass fraction of the gel matrix will not become zero. Due to this property, the feed-phase/active-layer system is much more like a liquid/gel system than a liquid/liquid system. Consequently, for a gel phase, activities are modeled in analogy to the models presented by Maurer and Prausnitz (1996) and Thiel et al. (1995):

$$\ln a_i = \ln a_i^L(T, p, x) + \frac{\hat{v}_i^0}{RT}\left(\frac{\partial A^{mbr}}{\partial V}\right)_T. \tag{30}$$

Here, $a_i^L(T, p, x)$ is the activity in the gel phase at the pressure surrounding the gel. This term is calculated with the assumption that the gel phase behaves like a liquid phase at the surrounding pressure p. However, due to the elastic properties of the polymer matrix, the expansion of the gel leads to a higher pressure inside the gel. This influence is described by the second term, which corresponds to the elastic properties of the network.

Using mass-based activity coefficients (cf. Eq. 9) yields

$$\ln \gamma_i' = \ln \gamma_i'^L(T, p, w) + \frac{\hat{v}_i^0}{RT}\left(\frac{\partial A^{mbr}}{\partial V}\right)_T. \tag{31}$$

This model is applied to the swelling active layer of the membrane.

Using UNIQUAC to Model the ''Liquid Activities.'' Since in the first term of Eq. 31 the membrane phase is treated like a liquid, the UNIQUAC model can be used to calculate activity coefficients $\gamma_i'^L(T, p, n_i)$. The classic UNIQUAC model (Reid et al., 1987) is converted to be used with mass fractions as follows:

$$\ln \gamma_i'^L = \ln \frac{\Phi_i}{w_i} + \frac{z}{2} q_i \ln \frac{\Theta_i}{\Phi_i} + l_i - r_i \sum_k \Phi_k \left[\frac{z}{2}\left(1 - \frac{q_k/M_k}{r_k/M_k}\right) - \left(1 - \frac{1}{r_k}\right)\right] + q_i' \left(1 - \ln \sum_{k=1}^{C} \Theta_k' \tau_{k,i} - \sum_{k=1}^{C} \frac{\Theta_k' \tau_{i,k}}{\sum_{m=1}^{C} \Theta_m' \tau_{m,k}}\right) \tag{32}$$

$$z = 10 \tag{33}$$

$$l_i = \frac{z}{2}(r_i - q_i) - (r_i - 1) \tag{34}$$

$$\tau_{i,j} = e^{u_{i,j}/T} \tag{35}$$

$$\Phi_i = \frac{w_i \dfrac{r_i}{M_i}}{\displaystyle\sum_{k=1}^{C} w_k \frac{r_k}{M_k}} \tag{36}$$

$$\Theta_i = \frac{w_i \dfrac{q_i}{M_i}}{\displaystyle\sum_{k=1}^{C} w_k \frac{q_k}{M_k}} \tag{37}$$

$$\Theta'_i = \frac{w_i \dfrac{q'_i}{M_i}}{\displaystyle\sum_{k=1}^{C} w_k \frac{q'_k}{M_k}}. \tag{38}$$

Since the PVA polymer chains of the active layer are large, they have a very high specific molecular size r_M, specific molecular surface q_M, and molecular weight M_M. However, in the preceding formulation only r_M/M_M, q_M/M_M (which are independent of the chain length), and $1/r_M$ (which can be set to zero for long chains) are needed for all components [parameters r_i and q_i are used in Eq. 34 only; since activity coefficients are not needed for the membrane material (see the section titled ''Boundary Conditions''), Eq. 34 is not used for the membrane material]. Since the PVA chains can be seen as being built up from ethanol molecules (Stephan, 1996), data taken from component ethanol are used for r_M/M_M and q_M/M_M.

Elastic Properties of the Network. Maurer and Prausnitz (1996) present different formulations for the second term of Eq. 31 based on the affine network theory and the phantom theory (Flory, 1953). In our case, however, these formulations gave only poor results when fitted to experimental data.

To derive an alternative semiempiric equation for the second term in Eq. 31, the polymer network is modeled by an elastic cube that changes its volume under pressure:

$$\frac{\hat{v}_i}{RT}\left(\frac{\partial A^{mbr}}{\partial V}\right) = \frac{\hat{v}_i^0}{k}\Phi^{2/3}(\Phi^{-1/3} - 1) = K_i^{mbr}\Phi^{2/3}(\Phi^{-1/3} - 1), \tag{39}$$

where

$$\Phi = \frac{V_0}{V} \tag{40}$$

is the volume fraction of the polymer, V is the volume of the swollen polymer, V_0 is the volume of the polymer at preparation time in an unswollen and dry state, and K_i^{mbr} is an empiric constant that represents the elastic properties of the polymer network.

In the case considered, this formulation gave the best results when fitted to experimental data and is thus used in Eq. 31.

Activities in the Supporting Layer. The activity of the vapor phase (the activity of a *hypothetical* liquid phase that would be in equilibrium with this vapor phase) is calculated by

$$a_i^V(y, p, T) = \frac{py_i}{p_i^0(T)}. \tag{41}$$

Density. The specific molar volume of a mixture is given by

$$\bar{v} = \sum_{i=1}^{C} x_i \bar{v}_i^0 + \bar{v}^M, \tag{42}$$

with

$$\bar{v}^M = RT \sum_{i=1}^{C} x_i \left(\frac{\partial \ln \gamma_i}{\partial p}\right)_{T,x}. \tag{43}$$

Since, according to Eqs. 31–39 the activities do not depend on the system pressure p for a liquid or a gel phase, $\bar{v}^M$ is zero. Thus, using mass fractions, the specific volume becomes

$$\bar{v} = \sum_{i=1}^{C} w_i \hat{v}_i^0, \tag{44}$$

and the total density can be calculated by

$$\rho_t(w, T) = \frac{1}{\displaystyle\sum_{i=1}^{C} w_i \hat{v}_i^0}. \tag{45}$$

Diffusion Coefficients. It is assumed that the friction between a dissolved molecule (E or Wd) and any embedded molecule We or polymer matrix M is the same:

$$Đ'_{M,E} = Đ'_{We,E}, \tag{46}$$

$$Đ'_{M,Wd} = Đ'_{We,Wd}, \tag{47}$$

Since the molecules cannot move relative to the polymer structure in the embedded mode, the corresponding diffusion coefficient is zero:

$$Đ'_{M,We} = 0. \tag{48}$$

To described the influence of the swelling state on the diffusive fluxes in the dissolved mode, the diffusion coefficients are calculated as functions of the number of molecules of water embedded in the polymer structure (w_{We}). In addition, an Arrhenius formulation is used to describe the temperature dependence of the diffusion coefficients (Reid et al., 1987):

$$Đ'_{Wd,E} = Đ^0_{Wd,E} \exp\left[K^{Arr}_{Wd,E}\left(\frac{1}{T_0} - \frac{1}{T}\right)\right] \tag{49}$$

$$Đ'_{M,E} = Đ^0_{m,E}(1 + K_E w_{We}) \exp\left[K^{Arr}_{M,E}\left(\frac{1}{T_0} - \frac{1}{T}\right)\right] \tag{50}$$

$$Đ'_{M,Wd} = Đ^0_{M,Wd}(1 + K_W w_{We}) \exp\left[K^{Arr}_{M,Wd}\left(\frac{1}{T_0} - \frac{1}{T}\right)\right]. \tag{51}$$

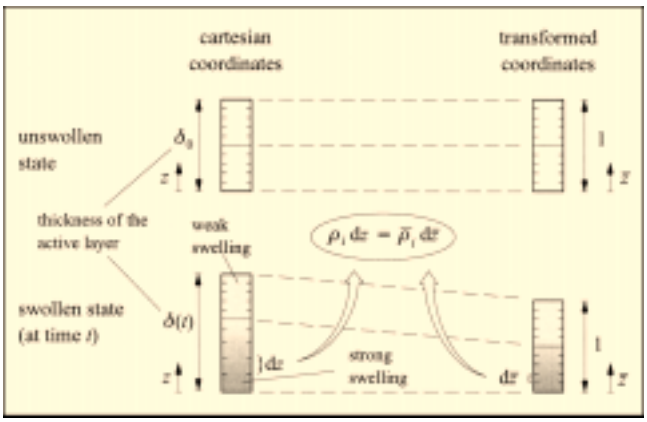

Figure 3. Coordinate transformation.

Model Transformation and Solution Method

Since the thickness of the active layer changes with time through the dissolution and embedding of molecules, the calculation domain also changes. This leads to a moving boundary problem that is difficult to solve.

To remedy this problem, a transformation of the coordinate z similar to the transformation proposed by Wu and Peppas (1993) is used. Coming from a ''dry'' and unswollen membrane, a dimensionless length with respect to its thickness is defined. Now, as depicted in Figure 3, each position on the swollen membrane can be related to the corresponding position on the unswollen membrane. This position $\bar{z}$ on the unswollen membrane is used as a transformed coordinate that will always be in the interval [0,1]. Note that the transformed coordinate $\bar{z}$ is not simply a specific length, that is, $z/\delta(t)$. Such a normalization would render the system of equations very difficult to solve. The transformation used leads to a relatively simple structure of equations that has a completely diffusive character, which corresponds to the quality of the physical problem.

For the mathematical formulation, the transformed density $\bar{\rho}_i$ is introduced in addition to the transformed coordinate $\bar{z}$. Obviously, these quantities must be related by the condition $\bar{\rho}_i\ d\bar{z} \equiv \rho_i\ dz$, since the amount of matter in a differential volume element must be independent of the coordinates used. Continuity for component M must also hold in the transformed coordinates. Hence

$$\frac{\partial \bar{\rho}_M}{\partial t} = -\frac{\partial\left(\bar{\rho}_M \bar{u}_M\right)}{\partial \bar{z}}. \tag{52}$$

Since the velocity of the membrane material $\bar{u}_M$ in the transformed coordinates is zero by definition, $\bar{\rho}_M$ does not change with time. In addition, the density of the unswollen membrane at some time t_0 is uniform, and thus $\bar{\rho}_M$ is a constant.

In order to apply the coordinate transformation to the whole set of equations, the following conditions are used:

$$\bar{\rho}_i\ d\bar{z} = \rho_i\ dz, \tag{53}$$

$$\bar{\rho}_M = \text{const}. \tag{54}$$

It follows from Eq. 53 for the membrane component that

$$\frac{\partial z}{\partial \bar{z}} = \frac{\bar{\rho}_M}{\rho_M} = \frac{\bar{\rho}_M}{w_M \rho_t}. \tag{55}$$

Equation 53 holds for each component, and also for the total density. Using Eq. 55 yields

$$\bar{\rho}_i = \rho_i \frac{\partial z}{\partial \bar{z}} = w_i\,\rho_t \frac{\bar{\rho}_M}{w_M \rho_t} = w_i \frac{\bar{\rho}_M}{w_M}, \tag{56}$$

$$\bar{\rho}_t = \rho_t \frac{\partial z}{\partial \bar{z}} = \rho_t \frac{\bar{\rho}_M}{w_M \rho_t} = \frac{\bar{\rho}_M}{w_M}. \tag{57}$$

Using Eqs. 56, 57 the mass fraction of component i can be shown to be the same in both the transformed and untransformed coordinates:

$$\bar{w}_i = \frac{\bar{\rho}_i}{\bar{\rho}_t} = \frac{w_i \dfrac{\bar{\rho}_M}{w_M}}{\dfrac{\bar{\rho}_M}{w_M}} = w_i. \tag{58}$$

The embedding rate in a physical element must be independent from the coordinate system used:

$$\bar{r}_i\ d\bar{z} = r_i\ dz. \tag{59}$$

This results in

$$\bar{r}_i = r_i \frac{\partial z}{\partial \bar{z}} = r_i \frac{\bar{\rho}_M}{w_M \rho_t}. \tag{60}$$

The transformation of the velocities is somehow more complicated. Integration of Eq. 53 for component M leads to

$$\bar{z}(t,z) = \frac{1}{\bar{\rho}_M} \int_0^z \rho_M(t,\zeta)\ d\zeta. \tag{61}$$

The transformed velocity $\bar{u}_i$ of a particle at position $\bar{z}_i[t, z_i(t)]$ can now be calculated from Eq. 61:

$$\bar{u}_i = \frac{d\bar{z}_i\left[t, z_i(t)\right]}{dt} = \frac{d}{dt}\left[\frac{1}{\bar{\rho}_M} \int_0^{z_i(t)} \rho_M(t,\zeta)\ d\zeta\right], \tag{62}$$

which, by means of Leibnitz rule (Bird et al., 1960), results in

$$\bar{u}_i = \frac{1}{\bar{\rho}_M}\left[\int_0^{z_i} \frac{\partial \rho_M(t,z)}{\partial t} dz + \rho_M(t,z_i) u_i(t,z_i)\right]. \tag{63}$$

After inserting Eq. 52, the integral can be solved to give

$$\bar{u}_i = \frac{1}{\bar{\rho}_M}\Big\{-\left[\rho_M(t,z_i) u_M(t,z_i) - \rho_M(t,0) u_M(t,0)\right] + \rho_M(t,z_i) u_i(t,z_i)\Big\}. \tag{64}$$

Since the coordinate system is fixed at $z = 0$ (beginning of the active layer), the velocity of the membrane $u_M(t,0)$ is always zero. Thus,

$$\bar{u}_i = \frac{1}{\bar{\rho}_M}\left[-\rho_M(t,z_i)u_M(t,z_i) + \rho_M(t,z_i)u_i(t,z_i)\right] = (u_i - u_M)\frac{\rho_M}{\bar{\rho}_M}. \quad (65)$$

Consequently the fluxes are given as

$$\bar{n}_i = \bar{w}_i\,\bar{\rho}_t\,\bar{u}_i = w_i\frac{\bar{\rho}_M}{w_M}(u_i - u_M)\frac{w_M\rho_t}{\bar{\rho}_M} = w_i\,\rho_t(u_i - u_M). \quad (66)$$

The fluxes $\bar{n}_i$ are calculated from the Maxwell-Stefan equation (cf. Eq. 13):

$$\left(\mathbf{\Gamma}_i\cdot\frac{\partial w}{\partial z}\right) = -\sum_{k=1}^{C}\frac{w_k\bar{n}_i - w_i\bar{n}_k}{\rho_t\mathcal{D}'_{i,k}}, \qquad i = 1\ldots C. \quad (67)$$

Converting to matrix notation yields

$$-\frac{1}{\rho_t}\left[B\cdot\bar{n}\right] = \left[\mathbf{\Gamma}\cdot\frac{\partial w}{\partial z}\right]. \quad (68)$$

Note that matrices B and $\mathbf{\Gamma}$ are the same as in Eqs. 14. As mentioned earlier for the fluxes j, this set of equations is also linearly dependent. Using the defining Eq. 66 for the flux $\bar{n}_M$, the following equation replaces the last row of Eq. 68

$$\bar{n}_M = w_M\,\rho_t(u_M - u_M) = 0 \quad (69)$$

(there is no flux of the membrane material in the transformed coordinates). Inverting this linear set of equations gives

$$\bar{n} = -\left[\bar{D}^{GMS}\cdot\frac{\partial w}{\partial z}\right] = -\frac{\rho_t}{\bar{\rho}_t}\left[\bar{D}^{GMS}\cdot\frac{\partial w}{\partial \bar{z}}\right]. \quad (70)$$

Note that rows 3 (We) and 4 (M) of matrix $\bar{D}^{GMS}$ contain zeros only, since there is no diffusional flux of water in the embedded mode (We) and of the membrane matrix (M).

Now, we have formulations to calculate all transformed variables from the physical variables. In the next step, balances are stated in transformed variables and the formulations derived earlier are inserted

$$w_E\frac{\partial\bar{\rho}_t}{\partial t} + \bar{\rho}_t\frac{\partial w_E}{\partial t} - \frac{\partial\bar{n}_E}{\partial\bar{z}} = 0, \quad (71)$$

$$w_{Wd}\frac{\partial\bar{\rho}_t}{\partial t} + \bar{\rho}_t\frac{\partial w_{Wd}}{\partial t} - \frac{\partial\bar{n}_{Wd}}{\partial\bar{z}} = -\frac{\bar{\rho}_t}{\rho_t}k_W(a_{Wd} - a_{We}), \quad (72)$$

$$w_{We}\frac{\partial\bar{\rho}_t}{\partial t} + \bar{\rho}_t\frac{\partial w_{We}}{\partial t} = \frac{\bar{\rho}_t}{\rho_t}k_W(a_{Wd} - a_{We}), \quad (73)$$

$$w_M\frac{\partial\bar{\rho}_t}{\partial t} + \bar{\rho}_t\frac{\partial w_M}{\partial t} = 0, \quad (74)$$

$$0 = w_M\,\bar{\rho}_t - \bar{\rho}_M. \quad (75)$$

Introducing the vector of unknowns $u = (w_E, w_{Wd}, w_{We}, w_M, \bar{\rho}_t)^T$, this system of equations can be rewritten in general form:

$$\left[B(\bar{z},t,u)\cdot\frac{\partial u}{\partial t}\right] - \frac{\partial}{\partial\bar{z}}\left[D(\bar{z},t,u)\cdot\frac{\partial u}{\partial\bar{z}}\right] = F(\bar{z},t,u). \quad (76)$$

Systems of this kind can be directly solved by KARDOS (Lang, 1996), an adaptive PDE solver.

Fitting of Model Parameters

The activity model (Eqs. 31–39) has five unary parameters for each component (r_i/M_i, q_i/M_i, q'_i/M_i, υ_i^0, and K_i^{mbr}) and one binary parameter for each pair of components ($u_{i,j}$). While the unary parameters r_i/M_i, q_i/M_i, q'_i/M_i, and υ_i^0 can be taken from the literature, the parameter K_i^{mbr} and the binary parameters $u_{i,j}$ (16 parameters in total) are determined by fitting the model to experimental sorption data for PVA/ethanol/water taken from Heintz and Stephan (1994a). Figure 4 shows that reasonable agreement is obtained, especially in the region with $w^L_{\text{ethanol}} > 0.7$, which is most significant for mass transfer. The resulting parameters can be found in Tables A1 and A2 in the Appendix.

The parameters of the transport model Eqs. 71–75, 70, 49–51 ($\mathcal{D}^0_{Wd,E}$, $\mathcal{D}^0_{M,E}$, $\mathcal{D}^0_{M,Wd}$, K_E, K_W, $K^{Arr}_{Wd,E}$, $K^{Arr}_{M,E}$, $K^{Arr}_{M,wd}$, and k_W) are now fitted to experimental mass-transfer data. In the first step, experimental mass-transfer data for the membrane Mo1140 (GFT, Neunkirchen, Germany), and taken from Franke (1990) are used. The parameters obtained from the fit can be found in Table A4 in the Appendix. Experimental and simulation data, which exhibit excellent agree-

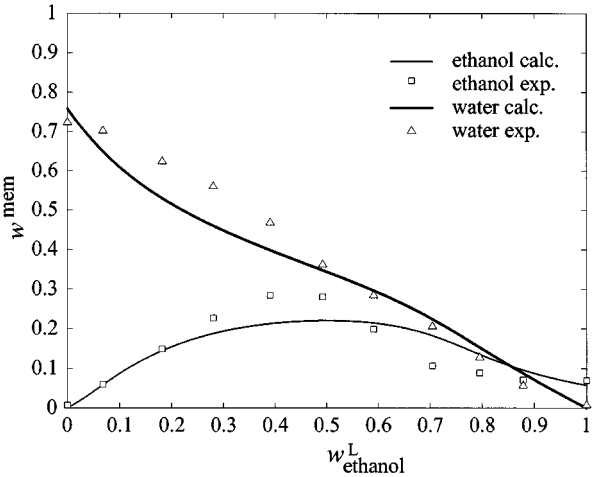

Figure 4. Sorption equilibrium between active layer of the membrane (PVA) and liquid feed phase at $t = 59.85$°C.

The amount of water adsorbed in both phases is w_W: $w_W = w_{Wd} + w_{We}$. Experimental data are taken from fig. 2 of Heintz and Stephan (1994a).

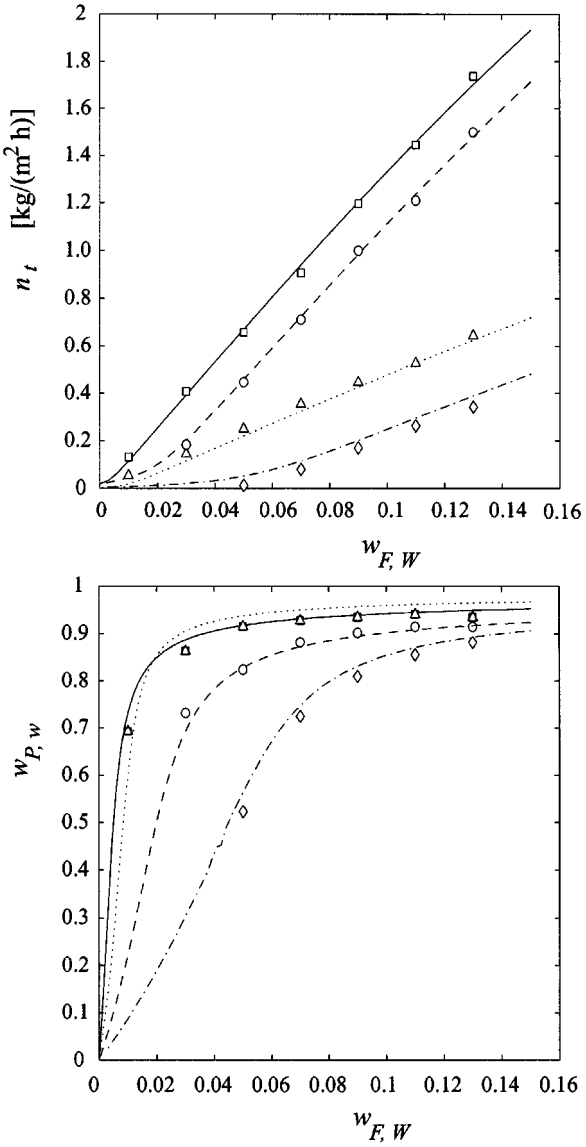

Figure 5. Membrane flux and permeate composition for the membrane Mo1140.

Experimental data (markers) and simulation results (lines) for steady state. □ — $p_P = 0.02$ bar, $t = 90$°C; ○ – – $p_P = 0.1$ bar, $t = 90$°C; △ ··· $p_P = 0.02$ bar, $t = 70$°C; ◇ – · – $p_P = 0.1$ bar, $t = 70$°C.

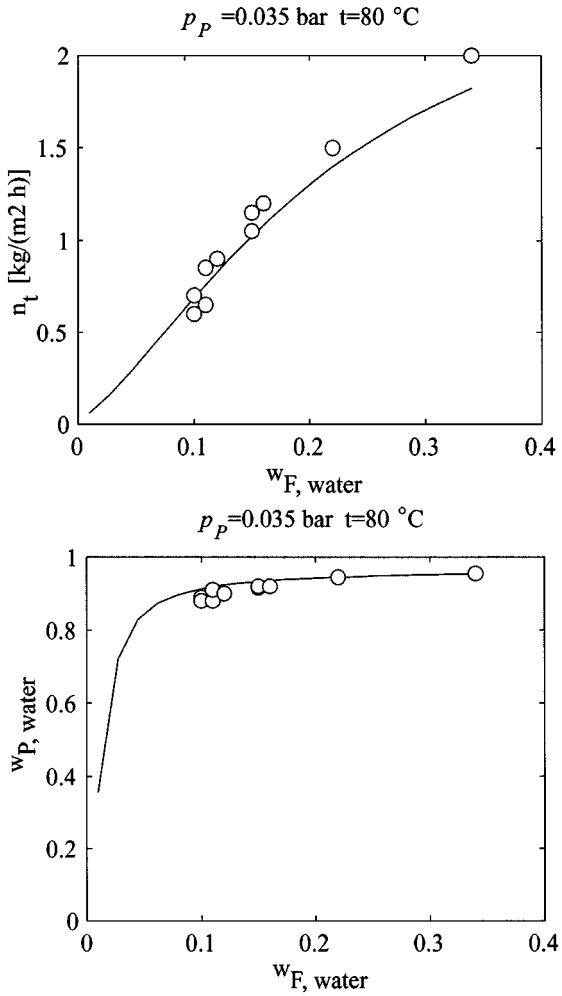

Figure 6. Membrane flux and permeate composition for the membrane PERVAP 1001 at $p_P = 0.035$ bar and $t = 80$°C.

Experimental data (markers) and simulation results (lines) for steady state.

ment, are shown in Figure 5. However, since only steady-state data are available for this membrane, the parameter k_W, which describes the kinetics of the embedding and dissolution process, could not be determined.

To fit parameters for the membrane PERVAP 1001 (Sulzer Chemtech GmbH, Winterthur, Switzerland) with the system ethanol/water experimental data from Hömmerich (personal communication, 1998) and Rautenbach and Hömmerich (1998) are used. In the first step, the steady-state parameters (all parameters except k_W) are fitted to the steady-state values of the experiments. However, these data show much higher experimental noise, as can be seen in Figures 6 and 7 and in the work of Rautenbach and Hömmerich (1998). Thus, there is some deviation between experimental and simulation data at steady state, especially in the fluxes.

In the next step, the kinetic parameter k_W is fitted to dynamic experimental data reported by the authors. The resulting parameters are listed in Table A4 in the Appendix.

Simulation Results

To illustrate the dynamic behavior of the model, simulations for a large step change of the feed composition from $w_{F,W} = 0.006$ to $w_{F,W} = 0.3$ are shown in Figures 8, 9, and 10.

Figure 8 shows the evolution of the thickness of the active layer on the left as a function of time. The lines correspond to virtual marks on the active layer that shift as a result of swelling. The position $z = 0$ is the feed side, where the swelling first occurs and is strongest. At $t = 0$ the feed composition changes, which results in a small but fast change in the thickness of the active layer after about 1 s.

After some minutes the process of embedding results in a higher mass fraction of water in the embedded mode. This

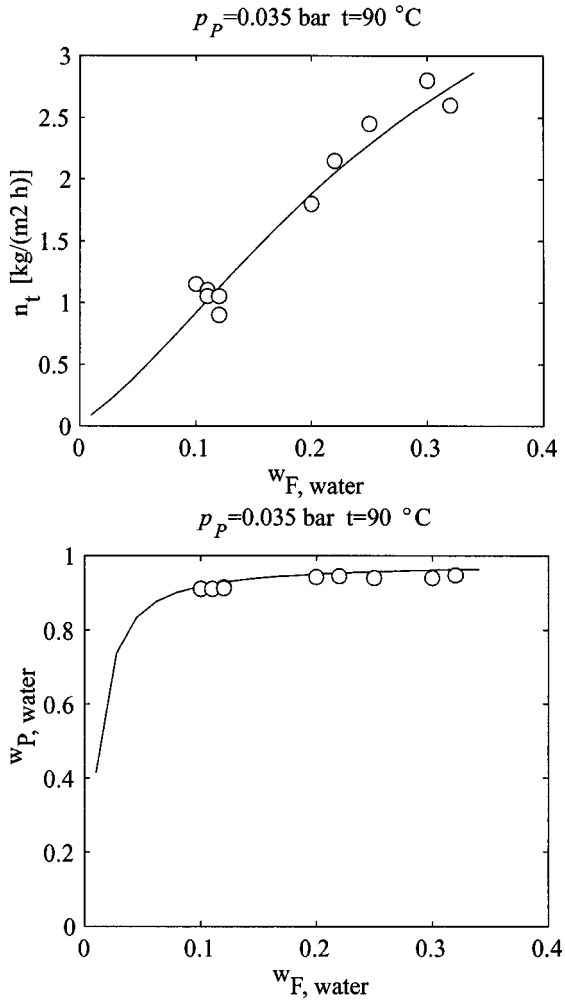

Figure 7. Membrane flux and permeate composition for the membrane PERVAP 1001 at $p_P = 0.035$ bar and $t = 90$°C.

Experimental data (markers) and simulation results (lines) for steady state.

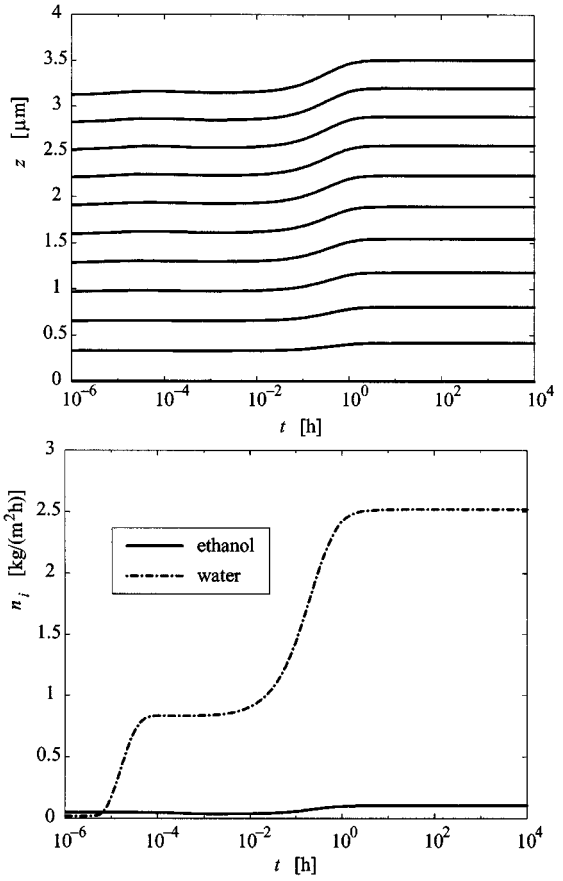

Figure 8. (Top) Change of the thickness of the active layer and (bottom) of the fluxes at $z = \delta(t)$.

The composition of the feed is changed at $t = 0$ from $w_{F,W} = 0.006$ to $w_{F,W} = 0.3$, $p_P = 0.03$ bar, $t_F = 90$°C. Note that a logarithmic scale is used for the time axis.

results in higher diffusion coefficients and fluxes, resulting in a second change in thickness and composition of the active layer. The final steady state is reached after some hours.

On the top of Figure 8, the membrane flux can be seen. The flux of water also increases after about 1 s, and increases again sharply after some minutes.

Figures 9 and 10 show the mass fraction of water in both the dissolved and embedded modes inside the active layer of the membrane. While w_{Wd} has reached a first quasi-stationary profile after about 1 s, w_{We} has not changed at all at this time, due to the slow embedding process. This shows that the time constant of the diffusion process alone, based on membrane thickness and diffusion coefficients, is very small. The swelling process is the time-determining step.

Through the coupling of embedding and diffusion, a two-step adaption to the changed feed conditions is described, which has been observed by Ping et al. (1988): when process conditions are changed, the diffusion process and thus the mass transfer are affected very quickly, due to the small time constant of the diffusion process. This leads to a first plateau in the flux vs. time diagram. The embedding process is much slower and affects mass transfer much later, however, resulting in a second plateau in the fluxes after some time.

A similar two-step adaption to changed conditions has been reported for swelling–dissolution in rubbery polymers using *in situ* NMR measurements (Devotta et al., 1994; Devotta et al., 1995a), and adsorption–diffusion in polymer solutions (Devotta et al., 1995b). It should be noted, however, that the physical phenomena causing the two-stage adaptation of the flux time history are markedly different from those considered in this article. In adsorption, fast formation of a condensed polymer film occurs quickly, which subsequently hinders transport into the pores, and thus leads to a plateau and a reduced increase of the flux. In dissolution, a polymer rich boundary layer forms rapidly, which again acts as a diffusion barrier and, after passing a plateau zone, results in reduced flux gradients. Instead, the two-stage adaptation of the membrane considered in this contribution is due to swelling and its implication on the diffusion of the dissolved monomer across the membrane film.

The dominant time constant of the mass-transfer model depends mainly on the kinetic parameter k_W. By tuning this

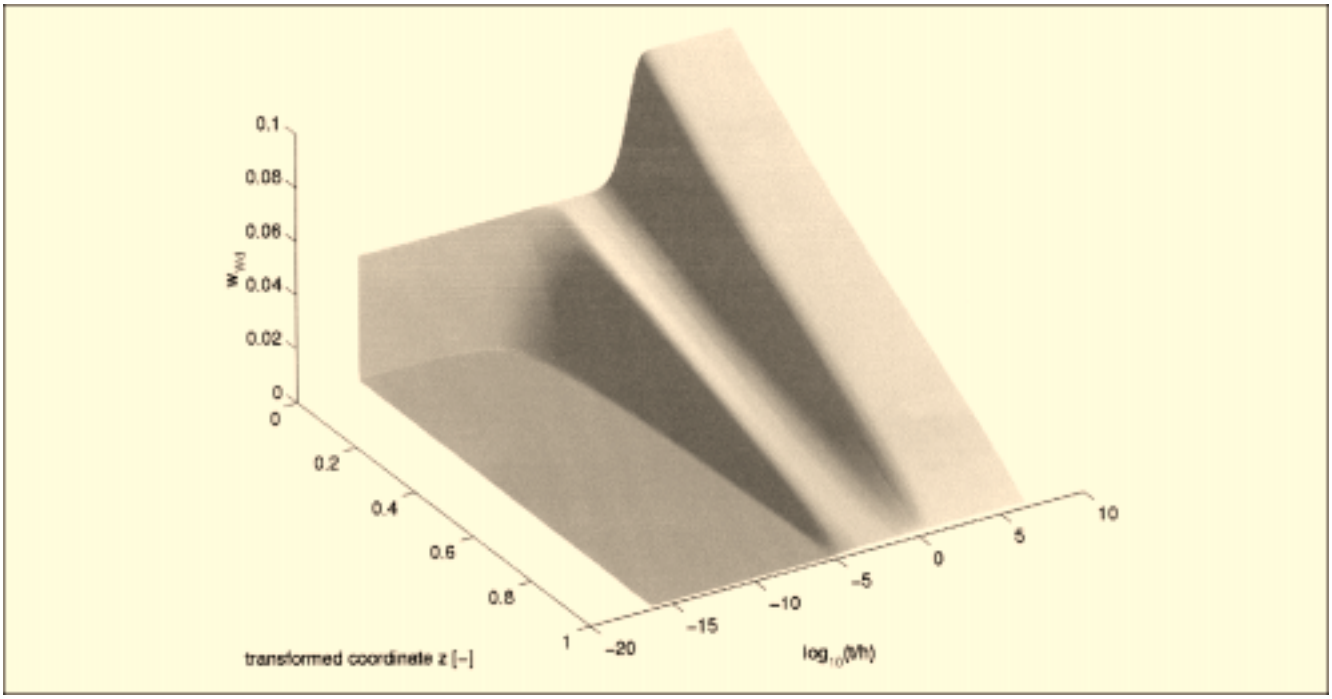

Figure 9. Mass fraction of water in the dissolved mode, $w_{Wd}(\bar{z},t)$.

parameter, the dynamic behavior of the model can be fitted to experimental data in a wide range of time constants. As can be seen in Figure 11, a high value of k_W leads to a fast swelling process and thus to a fast change in the fluxes. With $k_W = 100$ kg/(m^2·s), the dynamic behavior is mainly imposed by the fast diffusion process. When k_W is decreased, the swelling process gets slower, while the first step in the change of fluxes is not affected.

In Figure 12 experimental data taken from Rautenbach and Hömmerich (1998) and simulation results for a smaller step change in the feed composition are shown. As discussed in the section titled ''Fitting of Model Parameters,'' there is some deviation between experimental and simulation steady-state data for this membrane type (PERVAP 1001). Thus, the fluxes at steady state have a large deviation, especially before the first step change.

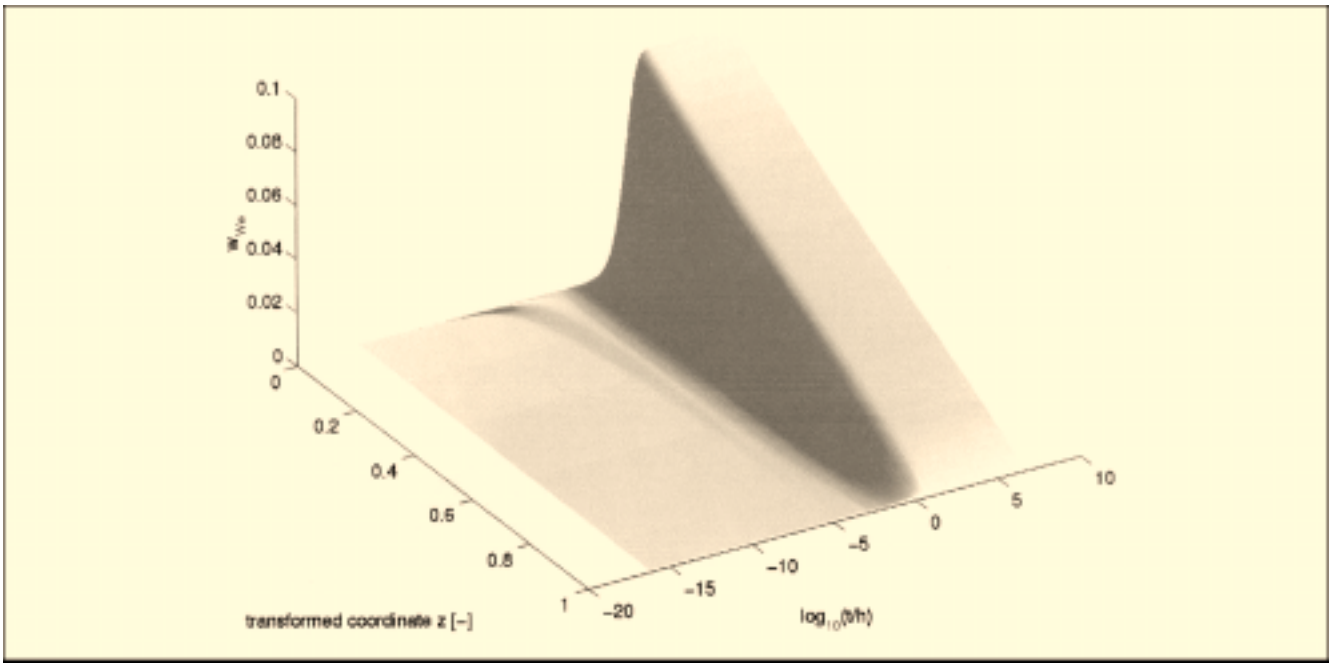

Figure 10. Mass fraction of water in the embedded mode, $w_{We}(\bar{z},t)$.

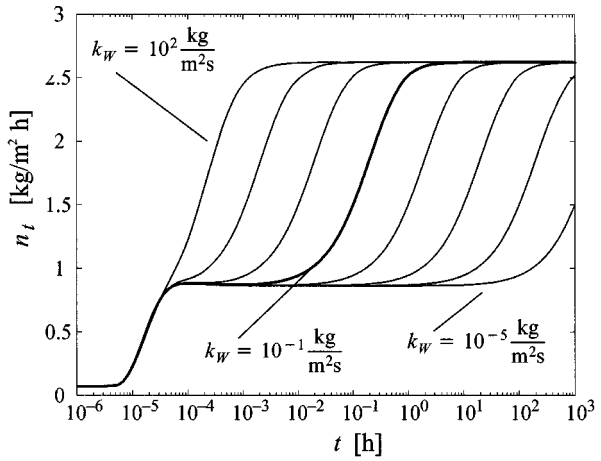

Figure 11. Dynamic total membrane flux for a variation of the kinetic parameter k_W.

However, the dynamic behavior of experimental and simulation data shows reasonable agreement. As illustrated in the last example, the first response of the membrane is very fast. In the simulation, the fluxes change with hardly any delay. Since in the experiment the first measurement is made 20 min after the change in the feed conditions, the observed gradient is smaller. After this first step, the fluxes take a longer time to reach steady state. At $t = 180$ min the feed composition switches back to the value before the first step. Again, the first response of the fluxes is very fast, while it takes a longer time to reach the steady state.

Figure 13 shows the dynamic response to the step change in feed composition for different step sizes. Figure 14 shows the dynamic response of the mass transfer for fast changes in the permeate pressure. When the permeate pressure is decreased, the concentration of water in the dissolved mode at interface Π decreases due to its smaller partial pressure in the permeate. This directly results in higher driving forces and fluxes. However, the smaller concentration of water in the dissolved mode leads, after some time, to a smaller concentration of water in the embedded mode. Since the diffusion coefficients increase with the mass fraction of water in the embedded mode, this results in a decrease in the fluxes after some time.

The reaction of mass transfer to a change in the feed temperature is shown in Figure 15. When the temperature is increased, the result is a higher vapor pressure at interface Π, and thus in a smaller "vapor activity" of both components (see Eq. 41). This results in higher driving forces and fluxes. Since the diffusion coefficients also increase with higher temperature (see Eqs. 49–51), the fluxes increase even more. Both effects are fast and result in a step change in the fluxes with nearly no time delay. Since the embedding/dissolution equilibrium is influenced weakly by temperature, the amount of water in the embedded mode remains nearly constant, and there is no slow adaptation of the flux, as in the previous cases.

Conclusions

Due to many publications, the slow adaption of mass-transfer rates in pervaporation to changing process conditions is

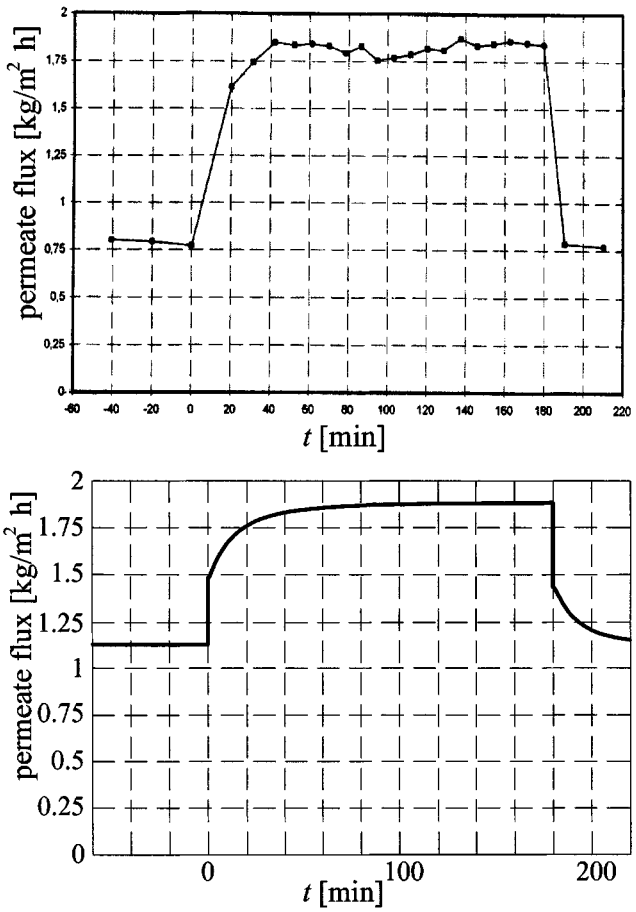

Figure 12. (Top) Experimental data taken from Rautenbach and Hömmerich (1998) and (bottom) simulation results.

Membrane flux for a change of feed composition from $w_{F,W} = 0.12$ to $w_{F,W} = 0.20$ at $t = 0$ ($p_P = 0.03$ bar, $t_F = 90°C$, PERVAP 1001).

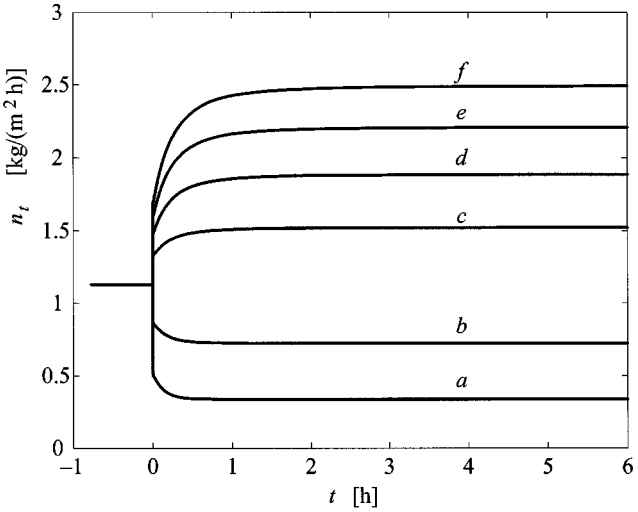

Figure 13. Membrane flux for a change of feed composition from (a) $w_{F,W} = 0.12$ to $w_{F,W} = 0.04$, (b) $w_{F,W} = 0.08$, (c) $w_{F,W} = 0.16$, (d) $w_{F,W} = 0.20$, (e) $w_{F,W} = 0.24$, and (f) $w_{F,W} = 0.28$ at $t = 0$ ($p_P = 0.03$ bar, $t_F = 90°C$, PERVAP 1001).

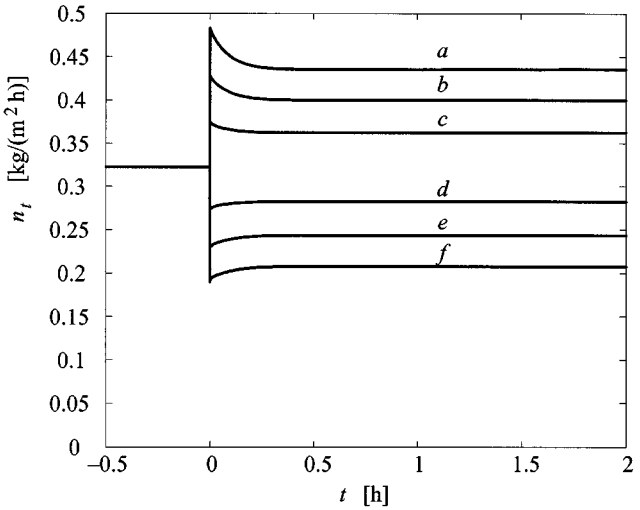

Figure 14. Membrane flux for a change of permeate pressure from (a) $p_P = 0.1$ bar to $p_P = 0.025$ bar, (b) $p_P = 0.05$ bar, (c) $p_P = 0.075$ bar, (d) $p_P = 0.125$ bar, (e) $p_P = 0.15$ bar, and (f) $p_P = 0.175$ bar at $t = 0$ ($w_{F,W} = 0.05$, $t_F = 90$°C, PERVAP 1001).

known. Until now this phenomenon has attracted little attention, and mostly qualitative experimental data are available. However, the time constants that have been reported have the same order of magnitude as the time constants of a pervaporation plant. Thus, the dynamic behavior of mass transfer may influence the whole process and should not be neglected when modeling pervaporation processes.

While mass-transfer models in the literature are not able to describe time constants of several minutes or hours, this article proposes a new mass-transfer model for pervaporation membranes. This model is based on the dual-sorption theory and Maxwell-Stefan fluxes. Through the tuning of the kinetic constant of the embedding process it is possible to describe either a very slow or a very fast dynamic behavior. Model parameters are fitted to both steady-state and dynamic experimental data. While it shows excellent agreement for the steady-state case, the dynamic behavior of mass transfer is also described. However, more and accurate dynamic data are needed to determine reliable values for all model parameters and to validate its applicability. After this step, in order to evaluate problems connected with dynamics and control, it may be integrated in dynamic plant models for pervaporation units of hybrid processes.

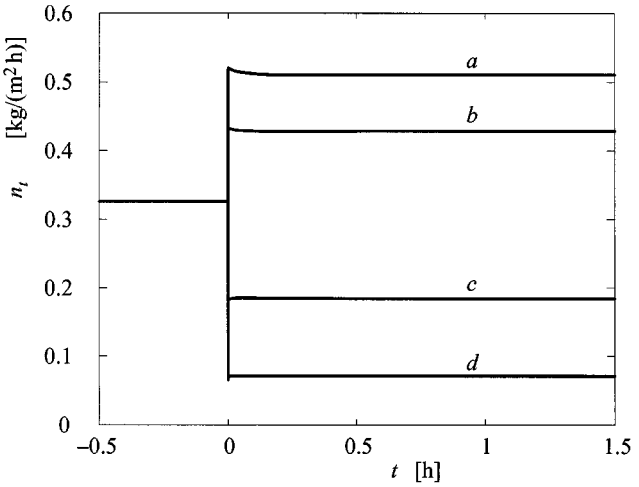

Figure 15. Membrane flux for a change of feed temperature from (a) $t_F = 80$°C to $t_F = 100$°C, (b) $t_F = 90$°C, (c) $t_F = 70$°C, and (d) $t_F = 60$°C at $t = 0$ ($w_{F,W} = 0.05$, $p_P = 0.03$ bar, PERVAP 1001).

The simulation studies with different step changes in Figures 13–15 show that the stationary gain does not depend on the step size, at least for small steps. It might thus be possible to identify simple linear models that can describe the mass transfer at some operating range. The high complexity of the model proposed in this article will result in a large-scale simulation problem when a whole pervaporation plant is addressed. On the other hand, simple linear models will lead to much smaller systems of equations that are much easier to handle.

Acknowledgment

This research was supported by the Volkswagen-Stiftung in the program ''Modellierung komplexer Systeme in der Verfahrenstechnik.''

Notation

Symbols

a_i = activity of component i
B = matrix function of inverted binary diffusion coefficients, s/m
A^{mbr} = elastic energy of the network, J/kmol
C = number of components
$Đ_{i,j}$ = Maxwell-Stephan diffusion coefficient with respect to moles, m^2/s
$Đ'_{i,j}$ = Maxwell-Stephan diffusion coefficient with respect to masses, m^2/s
$Đ^0_{i,j}$ = constant for concentration-dependent diffusion coefficients, m^2/s
D^{GMS} = matrix of Fick diffusion coefficients based on general Maxwell-Stefan equations in mass average velocity reference frame, m^2/s
$\overline{D}^{GMS}$ = matrix of Fick diffusion coefficients based on general Maxwell-Stefan equations relative to the membrane (transformed coordinates), m^2/s
j_i = mass diffusion flux of component i relative to the mass average velocity, kg/(m^2·s)
k = heat conductivity, W/(m^2·s·K)
k_W = constant for embedding kinetic of water, kg/(m^3·s)
K_i = constant for concentration-dependent diffusion coefficients, m^2/s
$K^{Arr}_{i,j}$ = Arrhenius constant for diffusion coefficient, m^2/s
K^{mbr}_i = elastic constant of the network
K^{pd} = pressure-drop constant
m_i = mass of component i, kg
n_i = mass flux of component i referred to a stationary coordinate reference frame, kg/(m^2·s)
n_t = mixture total mass flux referred to a stationary coordinate reference frame, kg/(m^2·s)
N_i = molar flux of component i referred to a stationary coordinate reference frame, kmol/(m^2·s)
N_t = mixture total molar flux referred to a stationary coordinate reference frame, kmol/(m^2·s)
N^c = molar flow through one capillary, kmol/s

$\bar{n}_i$ = mass diffusion flux of component i relative to the membrane, kg/(m^2·s)
p = pressure, N/m^2
p_i^0 = vapor pressure of component i, N/m^2
r = pore radius, m
r_i = rate of embedding of component i into the polymer structure, kg/(m^3·s)
R = gas constant, J/(kmol·K)
t = time, s
t = temperature, °C
T = temperature, K
u_i = velocity of species i, m/s
v = mass average velocity, m/s
$\hat{v}$ = specific volume of mixture, m^3/kg
$\hat{v}_i^0$ = specific volume of component i, m^3/kg
$\bar{v}$ = specific molar volume of mixture, m^3/kmol
$\bar{v}_i^0$ = specific molar volume of component i, m^3/kmol
w_i = mass fraction, kg/kg
x_i = mol fraction, kmol/kmol
z = coordinate, m
$\bar{z}$ = transformed coordinate

Greek letters

δ = thickness of the active layer, m
$\delta_{i,j}$ = Kronecker delta
δ_0 = thickness of the active layer of the dry membrane, m
δ^{SL} = thickness of the supporting layer, m
γ_i = activity coefficient of component i
γ_i' = activity coefficient of component i with respect to mass fractions ($\gamma_i' \equiv a_i/w_i$)
$\mathbf{\Gamma}$ = matrix of thermodynamic factors for Maxwell-Stefan fluxes
η = viscosity, N s/m^2
ϕ = area fraction of capillaries in the porous supporting layer
Φ = volume coefficient
ρ_i = mass density of component i, kg/m^3
$\bar{\rho}_i$ = transformed mass density of component i, kg/m^2
ρ_t = mixture mass density, kg/m^3
$\bar{\rho}_t$ = transformed mixture mass density, kg/m^3

Subscripts

E = ethanol
i = component i
I = connection feed/active layer
II = connection active layer/supporting layer
III = connection supporting layer/permeate
M = membrane
t = total
Wd = water (dissolved mode)
We = water (embedded mode)

Superscripts

0 = pure component
c = capillary
F = feed phase
L = liquid phase
M = membrane phase
P = permeate phase
V = vapor phase

Literature Cited

Bausa, J., and W. Marquardt, "Shortcut Design Methods for Hybrid Membrane/Distillation Processes for the Separation of Nonideal Multicomponent Mixtures," *Ind. Eng. Chem. Res.*, **39**(6), 1658 (2000).

Bird, R. B., W. E. Stewart, and E. N. Lightfoot, *Transport Phenomena*, Wiley, New York (1960).

Devotta, I., M. V. Badiger, P. R. Rajamohanan, S. Ganapathy, and R. A. Mashelkar, "Unusual Retardation and Enhancement in Polymer Dissolution: Role of Disengagement Dynamics," *Chem. Eng. Sci.*, **50**(16), 2557 (1995a).

Devotta, I., D. D. Ravetkar, V. D. Ambeskar, and R. A. Mashelkar, "A New Phenomenological Model for Adsorption-Diffusion in Polymer Solutions: Role of Disengagement Dynamics," *Chem. Eng. Sci.*, **50**(7), 1129 (1995b).

Devotta, I., V. Premnath, M. V. Badiger, P. R. Rajamohanan, S. Ganapathy, and R. A. Mashelkar, "On the Dynamics of Mobilization in Swelling-Dissolving Polymeric Systems," *Macromol.*, **24**, 532 (1994).

Eaton, R. F., R. J. Roe, G. L. Wilkes, and A. Tobolsky, "Thermodynamics of Hydrophilic Polymer Membranes: The Degree of Swelling and Salt Partition Coefficient," *Proc. Coatings and Plastics Meeting*, Vol. 35, Amer. Chem. Soc., p. 503 (1975).

Flory, J. P., *Principles of Polymer Chemistry*, Cornell Univ. Press, Ithaca, New York (1953).

Franke, M., *Auslegung und Optimierung von Pervaporationsanlagen zur Entwässerung von Lösungsmitteln und Lösungsmittelgemischen*, PhD Thesis, Aachen Univ. of Technology, Aachen, Germany (1990).

Heintz, A., and W. Stephan, "A Generalized Solution−Diffusion Model of the Pervaporation Process Through Composite Membranes—Part I: Prediction of Mixture Solubilities in the Dense Active Layer Using the UNIQUAC Model," *J. Memb. Sci.*, **89**, 143 (1994a).

Heintz, A., and W. Stephan, "A Generalized Solution-Diffusion Model of the Pervaporation Process Through Composite Membranes—Part II: Concentration Polarization, Coupled Diffusion and the Influence of the Porous Support Layer," *J. Memb. Sci.*, **89**, 153 (1994b).

Helget, A., M. Groebel, and E. D. Gilles, "Dynamic Simulation for Plant and Control System Design," *Proc. PSE* '94, Seoul, Korea, p. 1111 (1994).

Hömmerich, U., R. Rautenbach, J. Bausa, and W. Marquardt, "Modellierung der Pervaporation als Grundlage eines modellgestützten Entwurfs hybrider Trennprozesse am Beispiel der MTBE-Produktion," *Tech. Rep.*, LPT-pro-1998-04, RWTH Aachen, Germany (1998); URL: http://www.lfpt.rwth-aachen.de.

Lang, J., *KARDOS—Kaskade Reaction Diffusion System*, Konrad-Zuse-Zentrum für Informationstechnik, Berlin (1996).

Marquardt, W., "Towards a Process Modeling Methodology," *Methods of Model-Based Control*, R. Berber, ed., NATO-ASI Ser. E, Applied Sciences, Vol. 293, Kluwer, Dordrecht, p. 3 (1995).

Mason, E. A., and A. P. Malinauskas, *Gas Transport in Porous Media:* The Dusty Gas Model, *Elsevier, Amsterdam* (1983).

Maurer, G., and J. Prausnitz, "Thermodynamics of Phase Equilibrium for Systems Containing Gels," *Fluid Phase Equil.*, **115**, 113 (1996).

Moganti, S., R. D. Noble, and C. A. Koval, "Analysis of a Membrane/Distillation Column Hybrid Process," *J. Memb. Sci.*, **93**, 31 (1994).

Peppas, N. A., and H. J. Moynihan, "Solute Diffusion in Swollen Membranes. IV. Theories for Moderately Swollen Networks," *J. Appl. Poly. Sci.*, **30**, 2589 (1985).

Pettersen, T., and K. M. Lien, "Design of Hybrid Distillation and Vapor Permeation Processes," *J. Memb. Sci.*, **99**, 21 (1995).

Ping, Z., Q. Nguyen, R. Clement, and J. Neel, "Time-Dependent Phenomena in Pervaporation: Influence of the Crystallinity of Dense Poly(vinyl alcohol) Membranes on Their Pervaporation Performance," *Proc. Int. Conf. Pervaporation Processes in the Chem. Ind.*, R. Bakish, ed., Nancy, p. 231 (1988).

Pressly, T. G., and K. M. Ng, "A Break-Even Analysis of Distillation-Membrane Hybrids," *AIChE J.*, **44,** 93 (1998).

Rautenbach, R., and R. Albrecht, "The Separation Potential of Pervaporation: 1. Discussion of Transport Equations and Comparison with Reverse Osmosis," *J. Memb. Sci.*, **25**, 1 (1985a).

Rautenbach, R., and R. Albrecht, "The Separation Potential of Pervaporation. Part 2: Process Design and Economics," *J. Memb. Sci.*, **25**, 25 (1985b).

Rautenbach, R., and U. Hömmerich, "Study of Dynamic Mass-Transfer Effects in Pervaporation," *AIChE J.*, **44,** 1210 (1998).

Reid, R. C., J. M. Prausnitz, and B. E. Poling, *The Properties of Gases & Liquids*, 4th ed., McGraw-Hill, New York (1987).

Stephan, W., *Entwicklung eines Modells zum Stofftransport durch porenfreie Polymermembranen und Durchführung von Pervaporationsexperimenten*, PhD Thesis, Univ. of Heidelberg, Heidelberg, Germany (1996).

Table A1. Model Parameters for Describing Activity Coefficients Inside Active Layer of Membrane

	r_i/M_i (kmol/kg)	q_i/M_i (kmol/kg)	q_i'/M_i (kmol/kg)	$\hat{v}_i^0$ (m^3/kg)	K_i^{mbr}
E	4.5702×10^{-2}	4.2804×10^{-2}	4.2804×10^{-2}	1.3445×10^{-3}	3.6
Wd	5.1054×10^{-2}	7.7691×10^{-2}	7.7691×10^{-2}	1.0427×10^{-3}	3.6
We	5.1054×10^{-2}	7.7691×10^{-2}	7.7691×10^{-2}	1.0427×10^{-3}	3.6
M	4.5702×10^{-2}	4.2804×10^{-2}	4.2804×10^{-2}	1.3445×10^{-3}	3.6

Taylor, R., and R. Krishna, *Multicomponent Mass Transfer*, Wiley, New York (1993).

Thiel, J., G. Maurer, and J. Prausnitz, "Hydrogele: Verwendungsmöglichkeiten und thermodynamische Eigenschaften," *Chem.-Ing.-Tech.*, **67**, 1567 (1995).

Vier, J., *Pervaporation azeotroper wäßriger und rein organischer Stoffgemische—Verfahrensentwicklung und -integration*, PhD Thesis, Aachen Univ. of Technology, Aachen, Germany (1995).

Vieth, W., J. Howell, and J. Hsieh, "Dual Sorption Theory," *J. Memb. Sci.*, **1**, 177 (1975).

Wu, J., and N. Peppas, "Modeling of Penetrant Diffusion in Glassy Polymers with an Integral Sorption Deborah Number," *J. Poly. Sci., Part B*: Polym. Phys., **31**, 1503 (1993).

Appendix: Model Parameters

Model parameters are shown in Tables A1–A4.

Table A2. Binary UNIQUAC Parameters $u_{i,j}$ for Describing Activity Coefficients Inside Active Layer of Membrane

$u_{i,j}$	*E*	*Wd*	*We*	*M*
E	—	4.0943×10^{2}	3.2724×10^{2}	-1.7558×10^{1}
Wd	-2.0088×10^{3}	—	-2.5179×10^{3}	-3.1353×10^{3}
We	-9.3783×10^{2}	5.4427×10^{2}	—	-3.4301×10^{3}
M	-3.6401×10^{2}	5.2719×10^{1}	1.4712×10^{1}	—

Table A3. Model Parameters for Simulation of a Mo1140 Membrane

i, *j*	$\mathcal{D}_{ij}^0$ (m^2/s)	K_j (m^2/s)	$K_{i,j}^{Arr}$ (K)
Wd, *E*	4.4643×10^{-9}	—	5160.5
M, *E*	3.9017×10^{-13}	270.0641	8839.9
M, *Wd*	4.2668×10^{-11}	15.7086	6011.3

$K^{pd} = 3.5152\times10^{7}$ ($m^2\cdot bar^2\cdot s$)/kmol

$T_0 = 363.15$ K

Note: The kinetic parameter k_W could not be determined due to the lack of dynamic experimental data.

Table A4. Model Parameters for Simulation of PERVAP 1001 Membrane

i, *j*	$\mathcal{D}_{i,j}^0$ (m^2/s)	K_j (m^2/s)	$K_{i,j}^{Arr}$ (K)
Wd, *E*	4.2426×10^{-11}	—	22041.4
M, *E*	9.5246×10^{-13}	33.0635	2994.8
M, *Wd*	2.1786×10^{-11}	52.2465	1381.1

$K^{pd} = 2.7160\times10^{10}$ ($m^2\cdot bar^2\cdot s$)/kmol

$k_W = 0.1$ ($kg\cdot m^3$)/s

$T_0 = 363.15$ K

Manuscript received May 1, 2000, and revision received Oct. 6, 2000.